The radio source count at 93.2 GHz from observations of 9C sources using AMI and CARMA

Matthew L. Davies,[1] Irina I. Stefan,[1] Rosie C. Bolton,[1,2] John M. Carpenter,[3]
Thomas M. O. Franzen,[4] Keith J. B. Grainge,[1,2]★ David A. Green,[1]
Michael P. Hobson,[1] Natasha Hurley-Walker,[5] Anthony N. Lasenby,[1,2]
Malak Olamaie,[1] Yvette C. Perrott,[1] Guy G. Pooley,[1] Julia M. Riley,[1]
Carmen Rodríguez-Gonzálvez,[1,6] Richard D. E. Saunders,[1,2] Anna M. M. Scaife,[7]
Michel P. Schammel,[1] Paul F. Scott,[1] Timothy W. Shimwell,[1,4] David J. Titterington,[1]
Elizabeth M. Waldram[1] and Imogen H. Whittam[1]

[1]*Astrophysics Group, Cavendish Laboratory, 19 J. J. Thomson Avenue, Cambridge CB3 0HE, UK*
[2]*Kavli Institute for Cosmology Cambridge, Madingley Road, Cambridge CB3 0HA, UK*
[3]*Department of Astronomy, California Institute of Technology, 1200 East California Boulevard, MC 249-17, Pasadena, CA 91125, USA*
[4]*CSIRO Astronomy and Space Science, ATNF, PO Box 76, Epping, NSW 1710, Australia*
[5]*International Centre for Radio Astronomy Research, Curtin Institute of Radio Astronomy, 1 Turner Avenue, Technology Park, Bentley, WA 6845, Australia*
[6]*Spitzer Science Center, California Institute of Technology, MS 220-6, Pasadena, CA 91125, USA*
[7]*School of Physics & Astronomy, University of Southampton, Highfield, Southampton SO17 1BJ, UK*

ABSTRACT

We present results from follow-up observations of a sample of 80 radio sources, originally detected as part of the 15.2-GHz Ninth Cambridge (9C) survey. The observations were carried out, close to simultaneously, at two frequencies: 15.7 GHz, using the Arcminute Microkelvin Imager (AMI) Large Array, and 93.2 GHz, using the Combined Array for Research in Millimeter-wave Astronomy (CARMA).

There is currently little direct information on the 90-GHz-band source count for $S \lesssim 1$ Jy. However, we have used the measured 15.7-to-93.2-GHz spectral-index distribution and 9C source count to predict the differential source count at 93.2 GHz as $26 \pm 4(S/\mathrm{Jy})^{-2.15}$ Jy^{-1} sr^{-1}; our projection is estimated to be most accurate for $10 \lesssim S \lesssim 100$ mJy.

Our estimated differential count is more than twice the 90-GHz prediction made by Waldram et al.; we believe that this discrepancy is because the measured 43-GHz flux densities used in making their prediction were too low. Similarly, our prediction is significantly higher than that of Sadler et al. at 95 GHz. Since our spectral-index distribution is similar to the 20-to-95-GHz distribution measured by Sadler et al. and used in making their prediction, we believe that the difference is almost entirely attributable to the dissimilarity in the lower frequency counts used in making the estimates.

Key words: surveys – galaxies: active – radio continuum: general.

1 INTRODUCTION

Knowledge of the 90-GHz radio source counts remains poor, owing to the observational difficulties in carrying out large-area blind surveys at such frequencies [de Zotti et al. (2010) provide a useful summary of available high-frequency counts]. Progress has been made recently using data from *Planck*, which has allowed complete 100-GHz source counts to be obtained for $S \gtrsim 1$ Jy (Planck collaboration 2011). Nevertheless, information about the 90-GHz-band source counts at lower flux densities is required.

In analysing data from cosmic microwave background (CMB) experiments, knowledge of high-frequency source counts is vital. For instance, the processing of data from *Planck* to allow separate component maps to be generated makes use of priors derived from assumed radio source counts (see, for example, Barreiro et al. 2006).

In addition, a statistical correction to the angular power spectrum of the CMB anisotropies, measured using *Planck*, is required to account for the power injected by discrete sources with flux densities below the level at which they can be identified during component separation.

Information about radio source counts will also be necessary for designing the next generation of high-resolution Sunyaev–Zel'dovich experiments, for which radio point sources will be a significant contaminant (see, for example, Knox, Holder & Church 2004). It is also useful for constraining theoretical models concerning the high-frequency radio source population and its evolution, such as those of de Zotti et al. (2005).

Knowledge of the 90-GHz count is important for the simulation and analysis of data from the Atacama Large Millimetre Array (ALMA), which is currently under construction. For example, the 90-GHz count for flux densities ∼20 mJy is required to predict the number of sources likely to be suitable for phase calibration of data from the telescope and is vital for estimating the confusion limit in deep observations of the ALMA fields.

The combination of smaller telescope fields of view and, for the majority of sources, decreasing source flux densities with increasing frequency means that it is very time consuming to conduct blind surveys for $\nu \gtrsim 30$ GHz using dish-based telescope technology. Obtaining a direct 90-GHz source count down to flux densities of tens of millijanskys would require a blind survey of hundreds of square degrees of sky. The observing time required for such a project, using a telescope such as the Combined Array for Research in Millimeter-wave Astronomy (CARMA), would be prohibitive.

Recently, however, estimates of the 90-GHz-band count at sub-jansky flux densities have been made by Waldram et al. (2007) and Sadler et al. (2008) by applying a measured spectral-index distribution to a known source count at a lower frequency. For example, Waldram et al. extrapolated the 15.2-GHz count, measured directly as part of the Ninth Cambridge (9C) survey of radio sources (Waldram et al. 2003, 2010), to 90 GHz using measured spectra for a sample of 9C sources. This allowed the 90-GHz count to be predicted to low flux densities, without requiring new extensive surveying.

The methods used by Waldram et al. and Sadler et al. are similar to those proposed by Kellermann (1964) and Condon (1984). There is good agreement, over their common flux density range (80 $\lesssim$ $S \lesssim$ 200 mJy), between the two predictions. The estimate of Sadler et al. was made on the basis of simultaneous 20- and 95-GHz observations, whereas that of Waldram et al. was made by extrapolating results from simultaneous 15-, 22- and 43-GHz measurements made by Bolton et al. (2004) to 90 GHz.

In this paper, results are presented from direct observations of a subset of sources from the sample of Bolton et al. (2004). The observations were carried out close to simultaneously using CARMA at 93.2 GHz and the Arcminute Microkelvin Imager (AMI; AMI Consortium: Zwart et al. 2008) Large Array (LA) at 15.7 GHz. Following the method of Waldram et al. (2007), the measured spectral-index distribution was applied to the 9C source count to predict the count at 93.2 GHz. The measured 15.7-to-93.2-GHz spectral-index, $\alpha^{93.2}_{15.7}$, distribution is assumed to be independent of flux density over the range of interest and is further assumed to be representative of a complete, flux-density-limited sample of sources detected at the lower frequency. These assumptions are discussed in Sections 6.2 and 8.1.

In Section 2, we discuss the source sample in more detail. In Sections 3, 4 and 5 the CARMA and AMI observations and data reduction, and the mapping of the data and the extraction of source flux densities, are outlined. In Section 6, the estimate of the 93.2-GHz source count is described. In Section 7, we place lower limits on the 93.2-GHz count. In Section 8, we compare our results to previous work. Finally, in Section 9 we summarize the main conclusions of this work.

2 THE SOURCE SAMPLE

The 15.2-GHz 9C survey, carried out using the Ryle Telescope (RT), was the first high-frequency radio source survey of significant extent and depth. It covers a total area of 520 deg^2 to a completeness limit of ≈25 mJy, with some smaller areas complete to 10 and 5.5 mJy.

The 9C survey was originally carried out to provide information about the radio sources in the survey fields of the CMB telescope the Very Small Array (Watson et al. 2003). To make the analysis of the CMB data more straightforward, these fields were selected to avoid bright sources. Consequently, there is a shortfall in the number of 9C sources with $S > 100$ mJy, which is, therefore, the upper completeness limit of the survey.

Bolton et al. (2004) conducted multifrequency (1.4, 4.8, 15.2, 22 and 43 GHz) follow-up observations of almost 200 sources, detected as part of the 9C survey, using the Very Large Array (VLA) and RT. These sources form two complete, 15.2-GHz samples: one of 124 objects, complete to 25 mJy, and the other of 70 sources, complete to 60 mJy. The sources are drawn from the catalogues of the 00, 09 and 15 h fields presented by Waldram et al. (2003).

In this paper, results are presented from 93.2-GHz observations of 80 9C sources from the samples of Bolton et al. The sources form two complete samples at 15.2 GHz. The first comprises 48 sources from the 00 h field and is complete between 25 and 100 mJy. The second contains 32 sources from the 15 h field and is complete between 35 and 100 mJy. No sources with flux densities below the lower completeness limit are included in either sample, although there are two sources with $S_{15.2} > 100$ mJy in the 00 h sample.

3 CARMA OBSERVATIONS AND DATA REDUCTION

The six 10.4-m diameter and nine 6.1-m diameter CARMA antennas were used to make 93.2-GHz observations of the sources in the 00 h field in nine days between 2008 August 18 and 2008 October 4, and of the sources in the 15 h field in nine days between 2009 June 14 and 2009 June 30. The observations of the sources were interleaved every 15 min with 3-min observations of a bright point source – 3C 454.3 (00 h field) or J1635+381 (15 h field) – for calibration. The data from 2009 June 22 were found to be anomalous and were therefore discarded. This resulted in the loss of one source, J1502+3753, from our sample – this source has not been included as one of the 80 sources mentioned above.

The MIRIAD (Sault, Teuben & Wright 1995) software package was used for reduction of the visibility data, including flagging data affected by shadowed antennas, poor weather or antenna malfunctions, manual flagging of data for which abnormally large steps in the phase or amplitude of the calibrator source were observed, and line and passband calibration implemented using UVEDIT, LINECAL and MFCAL. The procedure adopted for absolute flux density calibration differs for the two fields and is summarized below.

3.1 Absolute flux density calibration for the 00 h field

During each of our observing runs on the 00 h fields, we included a short observation of either Uranus or Neptune for absolute flux

calibration. These calibrations were applied to the data using the model contained within the MIRIAD program SMAFLUX derived from Weisstein's planetary model.[1] This assumes that Uranus and Neptune have brightness temperatures of 128 and 125 K, respectively, at 93.2 GHz. For comparison, *Wilkinson Microwave Anisotropy Probe* has reported mean brightness temperatures of 120 ± 4 and 142 ± 11 K at the same frequency for Uranus and Neptune, respectively (Weiland et al. 2011). We therefore allow for an overall 10 per cent systematic uncertainty in the 93.2-GHz CARMA flux density scale; we combine this in quadrature with our other errors such as thermal noise, which are independent, throughout the rest of this paper. 3C 454.3 is observed as the phase calibrator during each of the observing runs and we find that its flux density is stable within 2.5 per cent between 2008 August and October. As a result, it is concluded that the day-to-day scatter in the flux density measurements is small compared to the uncertainty in the overall flux density scale.

3.2 Absolute flux density calibration for the 15 h field

During each of our observing runs on the 15 h fields, we included a short observation of the Be-type star with stellar wind (outflow) MWC349 for absolute flux calibration, since neither Uranus nor Neptune was available at the time of our observations. MWC349 has been used as a flux calibrator by the Plateau de Bure interferometer (PdBI) for several years.

Rodriguez et al. (2007) compared MWC349 flux density measurements at 2 cm taken over a 22-yr time period between 1984 and 2006 with the VLA. The range covered by the four flux density measurements is 3.2 per cent. Tafoya et al. (2004) suggest that the flux density at 6 cm decreased by 4 per cent over a 14-yr period between 1982 and 1996.

We have adopted the PdBI model, which gives a predicted flux density of $S_\nu = 1.10(\nu/(87\,\text{GHz}))^{0.6}$ Jy; we therefore adopt a flux density of MWC349 of 1.15 Jy at 93.2 GHz. This is within 2 per cent of the power-law fit to the MWC 349 spectral distribution in Tafoya et al. (2004).

To check that this gives a consistent absolute calibration to our 00 h field, we use a cross-calibration[2] of MWC349 against Uranus made on 2009 June 23. Adopting a brightness temperature for Uranus of 128 K as above, we find a flux density for MWC349 of 1.16 Jy at 93.2 GHz; this is in very good agreement with the Plateau de Bure predicted value and gives us good confidence that our two fields have consistent absolute calibration. J1635+381 was observed for phase calibration during each observing run and we find that the source's flux density was stable to within 1 per cent throughout the period of the observations. Again day-to-day scatter in the flux density measurements is negligible compared to the overall flux density scale uncertainty.

4 AMI OBSERVATIONS AND DATA REDUCTION

The AMI LA was used to carry out observations of the 00 h-field sources between 2008 August 21 and 2008 August 24 and the 15 h-field sources between 2009 June 16 and 2009 June 20. Observations of the sources were interleaved every 10 min with 1-min phase-calibrator observations of 3C6 (J0015+3216; 00 h field) or

J1521+4336 (15 h field). The telescope was used to make observations of a single linear polarization (Stokes $I + Q$) between 13.5 and 18.0 GHz, with continuum flux densities being derived at 15.7 GHz. We do not expect the fact that we measure Stokes $I + Q$ with AMI and I with CARMA to affect our source count prediction, as any effect on individual spectral indices ought to average out for the sample as a whole.

The data were reduced using the in-house software, REDUCE; further detail about the calibration steps applied using REDUCE is given in AMI Consortium: Davies et al. (2009). Flux density calibration was carried out using regular observations of the AMI primary calibrator sources, 3C 286 and 3C 48; the flux densities assumed for these sources in each of the AMI frequency channels are given in AMI Consortium: Franzen et al. (2011).

5 MAPPING AND SOURCE FLUX DENSITIES

The AMI and CARMA data were mapped and CLEANed using the IMAGR task in AIPS[3] and an estimate of the rms noise on each of the maps was made using the IMEAN task. Each map was then multiplied to correct for the relevant telescope primary beam. A 'noise map', showing the variation in the noise level with position, was created for each map using the measured noise value and the relevant primary beam pattern. The maps and their corresponding noise maps were then output from AIPS as FITS images.

Source flux densities were extracted from the maps using the in-house software, SOURCEFIND, which is described in detail in AMI Consortium: Franzen et al. (2011). For most sources the peak value, calculated by interpolating between the map pixel values, provides the best flux density estimate. However, for sources that appear extended with respect to the synthesized beam, integrated flux densities were calculated. The integration area of a source was taken to consist of contiguous pixels down to a lowest contour level of $2.5\sigma_n$, where σ_n is the corresponding pixel value on the noise map.

The uncertainty in a flux density measured using the LA is assumed to consist of a calibration error (estimated at 5 per cent) added in quadrature with the noise at the position of the source (i.e. $\sqrt{(0.05S)^2 + \sigma_n^2}$), where S is the source flux density. For a flux density measured using CARMA, the quoted uncertainty consists of a 10 per cent error, arising from uncertainty in the overall CARMA flux density scale, added in quadrature with the thermal noise at the source position (i.e. $\sqrt{(0.1S)^2 + \sigma_n^2}$). The day-to-day scatter in the CARMA flux density measurements of a few per cent, mentioned in Section 3, is neglected, since it is small compared to the 10 per cent uncertainty in the overall flux density scale.

All sources were detected at 15.7 GHz with signal-to-noise ratios of at least 10. Of these, 70 were detected with peak flux densities $\geq 5\sigma_n$ using the CARMA data. A further seven sources were found to have peak flux densities $\geq 3\sigma_n$. The remaining three sources, J0018+3105, J0020+3152 and J0021+3226, were not detected at 93.2 GHz at the $3\sigma_n$ level. Table 1 shows the flux densities and $\alpha_{15.7}^{93.2}$ measured for each of the sources, along with their associated uncertainties. For each of the three sources that were not detected at 93.2 GHz, a 95 per cent upper bound on the flux density is given, which was used to calculate the quoted limiting spectral index.

---

[1] http://www.ericweisstein.com/research/thesis
[2] http://carma.astro.umd.edu/ tyu/FluxSource/FluxSource.cat

[3] http://www.aips.nrao.edu/index.shtml

Table 1. Measured 15.7-GHz and 93.2-GHz flux densities (mJy), and 15.7-to-93.2-GHz spectral indices for the sources in our sample, along with associated uncertainties. For the 93.2-GHz flux densities both the thermal, Tml, and total, Tot (including the overall absolute calibration uncertainty), errors are given. The estimate of the error in the spectral index uses only the thermal error in the 93.2-GHz flux density – the error in the overall 93.2-GHz flux scale is included in our result as a systemic error as described in Section 6.2. We assume that the spectral index error is $\sqrt{((\sigma_{15.7}/S_{15.7})^2 + (\sigma_{93.2}/S_{93.2})^2)}/\ln(93.2/15.7)$. For the three sources that were not detected at the higher frequency, limits on the 93.2-GHz flux density and spectral index are given.

Source	$S_{15.7}$	$\sigma_{15.7}$	$S_{93.2}$	$\sigma_{93.2}$ Tml	Tot	$\alpha_{15.7}^{93.2}$	σ_α	Source	$S_{15.7}$	$\sigma_{15.7}$	$S_{93.2}$	$\sigma_{93.2}$ Tml	Tot	$\alpha_{15.7}^{93.2}$	σ_α
J0002+2942	48.3	2.6	24.4	2.5	3.5	0.38	0.15	J0030+2809	26.1	1.5	10.7	3.4	3.6	0.50	0.42
J0003+2740	60.9	3.3	14.8	2.2	2.6	0.80	0.20	J0030+2833	43.1	2.6	4.6	0.5	0.7	1.26	0.16
J0003+3010	56.4	3.0	24.2	2.0	3.1	0.48	0.13	J0030+2957	25.7	1.4	19.9	1.9	2.8	0.15	0.14
J0005+3139	73.8	3.9	24.8	2.0	3.2	0.61	0.12	J0030+3415	17.5	1.1	7.2	0.5	0.9	0.50	0.12
J0010+2619	50.8	2.9	14.4	4.7	4.9	0.71	0.43	J0031+3016	39.9	2.1	14.4	1.6	2.2	0.57	0.16
J0010+2650	73.3	3.9	50.1	1.7	5.3	0.21	0.08	J0033+2752	18.8	2.1	5.9	0.9	1.1	0.65	0.24
J0010+2717	18.5	1.1	18.9	2.4	3.1	−0.01	0.18	J0034+2754	258.2	14.2	78.8	6.4	10.2	0.67	0.13
J0010+2838	43.7	2.3	53.5	5.1	7.4	−0.11	0.14	J0036+2620	42.1	2.2	9.3	1.8	2.0	0.85	0.25
J0010+2854	125.4	6.4	231.6	3.6	23.4	−0.34	0.07	J1502+3947	31.7	1.7	8.0	1.1	1.4	0.77	0.19
J0010+2956	50.4	2.6	21.9	3.6	4.2	0.47	0.22	J1502+3956	57.1	3.0	21.7	2.6	3.4	0.54	0.17
J0010+3403	24.3	1.3	4.8	1.0	1.1	0.91	0.28	J1503+4528	57.9	3.0	9.8	1.0	1.4	1.00	0.14
J0011+2803	36.3	2.2	9.6	0.7	1.2	0.74	0.12	J1510+3750	60.5	3.2	8.0	0.5	0.9	1.13	0.10
J0011+2928	45.6	2.4	12.3	1.5	1.9	0.74	0.17	J1510+4221	61.0	3.2	40.1	2.2	4.6	0.24	0.10
J0012+2702	58.5	3.1	10.1	0.9	1.4	0.98	0.14	J1511+4430	51.7	2.7	12.6	1.7	2.1	0.79	0.19
J0012+3053	11.8	0.7	9.8	2.9	3.0	0.10	0.39	J1514+3650	92.5	4.8	36.2	2.0	4.1	0.53	0.10
J0012+3353	134.9	6.9	151.9	8.7	17.5	−0.07	0.10	J1516+3650	65.9	3.7	56.4	2.7	6.2	0.09	0.10
J0013+2646	21.5	1.2	1.7	0.5	0.5	1.42	0.35	J1517+3936	98.7	5.1	74.4	2.7	7.9	0.16	0.08
J0013+2834	17.0	1.0	15.5	2.8	3.2	0.05	0.25	J1519+3913	43.8	2.3	8.9	0.7	1.2	0.89	0.13
J0014+2815	38.8	2.1	17.5	2.3	2.9	0.45	0.18	J1519+4254	36.4	1.9	26.0	2.2	3.4	0.19	0.13
J0015+3052	36.8	1.9	8.1	0.7	1.0	0.85	0.12	J1520+3843	37.2	1.9	11.0	1.4	1.8	0.68	0.17
J0015+3216	380.9	19.3	139.5	5.2	14.9	0.56	0.08	J1520+4211	43.0	2.2	115.5	3.2	12.0	−0.56	0.08
J0018+2907	23.8	1.3	17.3	1.8	2.5	0.18	0.15	J1523+4156	52.1	2.7	7.9	0.6	1.0	1.06	0.12
J0018+2921	88.0	4.6	34.9	4.1	5.4	0.52	0.17	J1525+4201	65.0	3.3	32.2	2.4	4.0	0.39	0.12
J0018+3105	19.8	1.2	<4.2	1.4	1.4	>0.87		J1526+3712	47.7	2.5	46.6	2.6	5.3	0.01	0.10
J0019+2647	57.5	3.1	54.2	2.6	6.0	0.03	0.09	J1526+4201	46.7	2.4	19.5	2.3	3.1	0.49	0.17
J0019+2817	20.1	1.2	46.9	2.7	5.4	−0.47	0.11	J1528+3738	86.2	4.4	13.5	1.4	1.9	1.04	0.15
J0019+2956	45.3	2.4	18.8	1.5	2.4	0.49	0.13	J1528+3816	78.1	4.0	53.6	2.5	5.9	0.21	0.09
J0019+3320	29.4	1.6	4.9	1.0	1.1	1.00	0.26	J1528+4219	42.5	2.2	23.5	1.1	2.6	0.33	0.09
J0020+3152	20.6	1.2	<2.1	0.7	0.7	>1.07		J1528+4522	38.6	2.0	37.5	2.5	4.5	0.02	0.11
J0021+2711	33.5	1.8	9.6	0.9	1.3	0.70	0.14	J1529+4538	36.7	1.9	8.6	0.4	1.0	0.82	0.09
J0021+3226	25.3	1.4	<3.0	1.0	1.0	>1.09		J1530+3758	57.2	3.0	9.7	0.8	1.3	1.00	0.13
J0022+3250	16.0	1.5	8.7	1.9	2.1	0.34	0.31	J1538+4225	45.9	2.4	50.2	2.8	5.8	−0.05	0.10
J0023+2734	62.8	3.2	20.5	1.5	2.6	0.63	0.12	J1541+4456	43.3	2.2	9.0	0.5	1.0	0.88	0.10
J0023+3114	30.1	1.6	9.2	1.3	1.6	0.66	0.20	J1545+4130	50.3	2.6	21.8	1.9	2.9	0.47	0.13
J0024+2911	58.8	3.0	122.8	2.3	12.5	−0.41	0.07	J1547+4208	75.8	3.9	35.2	1.4	3.8	0.43	0.08
J0027+2830	21.7	1.4	3.3	0.5	0.6	1.07	0.23	J1548+4031	102.9	5.3	29.6	2.9	4.1	0.70	0.14
J0028+2914	70.6	3.7	7.2	0.7	1.0	1.29	0.14	J1554+4348	41.7	2.2	16.2	1.3	2.1	0.53	0.13
J0028+2954	32.4	1.7	37.1	2.9	4.7	−0.08	0.12	J1554+4350	30.6	1.6	19.4	2.2	2.9	0.26	0.16
J0028+3103	45.6	2.4	4.9	0.9	1.1	1.25	0.26	J1556+4259	46.5	2.5	15.3	2.3	2.7	0.62	0.20
J0029+3244	37.8	2.1	7.0	1.4	1.5	0.95	0.26	J1557+4007	42.5	2.3	17.8	2.5	3.0	0.49	0.19

6 SOURCE COUNT ESTIMATE

6.1 Method

The measured 9C source count, and the 15.7- and 93.2-GHz flux densities of the sources have been used to estimate the 93.2-GHz source count, by application of the method described by Waldram et al. (2007). The flux density of each of the sources is assumed to vary with frequency according to a power law ($S \propto \nu^{-\alpha}$). It is further assumed that the sources in the sample have a typical distribution of spectral indices and that this distribution is independent of flux density.

Given the above assumptions, the source count at 93.2 GHz, $n_{\nu_2}(S) \equiv \mathrm{d}N_{\nu_2}/\mathrm{d}S$, can be estimated from the source count at 15.2 GHz, $n_{\nu_1}(S) \equiv \mathrm{d}N_{\nu_1}/\mathrm{d}S$, which is assumed to have a power-law dependence on flux density (i.e. $n_{\nu_1} = A_{\nu_1}S^{-b}$, where A_{ν_1}

and b are constants). Waldram et al. (2003) measured n_{ν_1} to be $51(S/\mathrm{Jy})^{-2.15}\,\mathrm{Jy}^{-1}\,\mathrm{sr}^{-1}$. Waldram et al. (2007) show that

$$n_{\nu_2} = Kn_{\nu_1} = KA_{\nu_1}S^{-b}, \qquad (1)$$

where

$$K = \frac{1}{m}\sum_{i=1}^{m} r_i^{(1-b)}, \qquad (2)$$

m is the number of sources in the sample and

$$r_i = \left(\frac{\nu_1}{\nu_2}\right)^{-\alpha_i} = \frac{S_{\nu_1}}{S_{\nu_2}}. \qquad (3)$$

We also define k_i such that
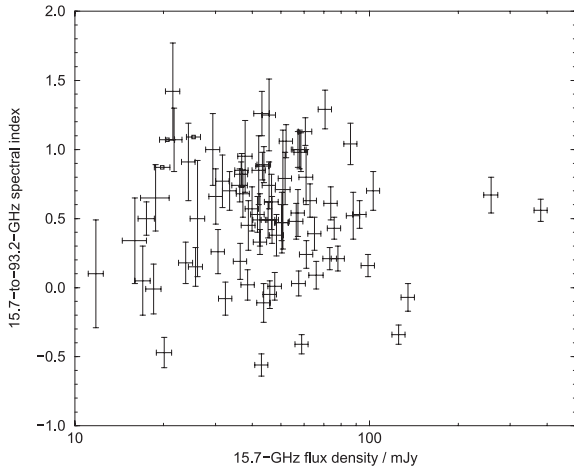
$$k_i = r_i^{(1-b)}. \qquad (4)$$

Figure 1. The 15.7-GHz flux densities of the sources versus their spectral indices. The three sources that were undetected at 93.2 GHz and for which the spectral indices were estimated as described in the text are indicated by open squares.

The measured flux densities were used to calculate the value of k for each source. For each of the three sources undetected at 93.2 GHz, an assumed value of k was calculated and was included in calculating K for the sample. To calculate the assumed value of k an upper bound, k_{max}, on k was first derived, using the limit on the flux density given in Table 1. The value of k for the source was then assumed to be equal to the median value of k for all sources that were measured to have $k \leq k_{max}$. Since only a small proportion of the sources were undetected at 93.2 GHz, estimating k in this way is likely to have little effect on the value of K.

6.2 Results

In calculating the k values for the sources, the small difference between the 9C survey frequency (15.2 GHz) and the frequency of the follow-up AMI observations (15.7 GHz) has been taken into account by assuming that the measured spectral indices hold over the additional frequency range. Therefore, the K parameter for the sample, calculated as 0.51 ± 0.06, compares the source count at 15.2 GHz with that at 93.2 GHz. This error estimate does not include any allowance for the overall 10 per cent systematic uncertainty in the 93.2-GHz flux density scale (see Section 3.1), which gives an additional fractional error of $(1 - b) \times 10$ per cent $= 11.5$ per cent to be combined in quadrature. Finally, the uncertainty in A_{ν_1} (the pre-factor in the 15.2-GHz source count) is also included in quadrature. This gives the projected 93.2-GHz count as $26 \pm 4(S/\text{Jy})^{-2.15}$ Jy^{-1} sr^{-1}.

The analysis above does not account for any uncertainty resulting from the assumption that the spectral index is independent of flux density (though no evidence for such a dependence is detected). Fig. 1 shows the value of $S_{15.7}$ plotted versus $\alpha_{15.7}^{93.2}$ for each of the sources; the 40 sources with the highest 15.7-GHz flux densities ($\gtrsim 45$ mJy) were found to have $\bar{\alpha}_{15.7}^{93.2} = 0.52 \pm 0.08$ and the remaining 40 sources to have $\bar{\alpha}_{15.7}^{93.2} = 0.54 \pm 0.09$.

7 LOWER LIMIT ON THE 93.2-GHZ SOURCE COUNT

In addition to our best estimate of the 93.2-GHz count, given in Section 6.2, we can place a lower limit on the source count at

Table 2. Lower limits on the 93.2-GHz differential source count from this work compared with predicted values from Section 6.2. In order to make a simple comparison, these counts are not normalized.

Bin start S (mJy)	Bin end S (mJy)	Number of sources	dN/dS measured (10^4 Jy sr^{-1})	dN/dS predicted (10^4 Jy sr^{-1})
1	2	1	2.5 ± 2.5	3501 ± 539
2	5	5	4.1 ± 1.8	623 ± 96
5	10	19	9.4 ± 2.2	110 ± 17
10	30	30	3.7 ± 0.7	16 ± 2.5
30	50	9	1.1 ± 0.4	2.8 ± 0.4
50	100	8	0.4 ± 0.14	0.8 ± 0.1
100	250	5	0.08 ± 0.04	0.1 ± 0.02

93.2 GHz. We calculate this lower limit by treating the measured 93.2-GHz flux densities as if they were derived from a blind survey at that frequency, rather than from pointed follow-up observations of a sample selected at a lower frequency.

Of course, were we to carry out such a blind survey, we would expect to detect many sources within our survey area for which we have not measured a 93.2-GHz flux density. This is because the sources in question did not appear in our lower frequency sample. For example, sources with flat or rising spectra might have large flux densities at 93.2 GHz but fall below the lower completeness limit at 15.2 GHz. We also recall that our sample has an upper completeness limit at the lower frequency, since the survey areas were selected to be free from sources with very large flux densities. Any such sources will be 'missing' from our 93.2-GHz sample.

In order to calculate this count we need to know the effective sky area. As explained in Section 2, the samples in this paper are drawn from the 9C multifrequency samples presented in Bolton et al. (2004). In the Bolton samples, a few of the 9C sources were missing but, since the omissions were totally unrelated to the source characteristics (i.e. they were due to scheduling problems), this meant simply that the effective sample areas were slightly reduced. The completeness of the samples in this paper is not affected and the effective areas can be estimated from the numbers of sources and the known 9C source count. The sample from the 00 h field is complete at 15.2 GHz between 25 and 100 mJy and contains 46 sources in this flux density range. Using the 9C source count, we estimate that the sample was derived from a sky area of 61 ± 9 deg^2. By similar reasoning, the 15 h sample is estimated to have been obtained from an area of 72 ± 13 deg^2, giving a total area of 133 ± 16 deg^2 for our entire sample.

The 77 sources detected at 93.2 GHz have been binned according to their flux densities at that frequency. By using the areas given above, we have calculated lower limits on the differential source count at 93.2 GHz for each of the flux density bins; these estimated lower limits to the counts are shown in Table 2, together with our best estimates from the projected count in Section 6.2. In order to make a simple comparison, these counts are not normalized. The results look very much as expected. In the lower bins, there are clearly large numbers of missing sources in the 'blind' count but at the high end the two counts converge.

8 DISCUSSION

8.1 Range of validity of our prediction

It is important to consider the flux density range over which the source count prediction given in Section 6.2 is valid. Following the

method of Waldram et al. (2007), it is possible to define an effective value of r for our sample, r_e, as

$$r_e = K^{1/(1-b)}. \qquad (5)$$

The flux density range over which the source count prediction is valid for ν_2 can be estimated using r_e and the properties of the source sample at ν_1. The minimum and maximum flux densities, S_{min} and S_{max}, over which the count is valid at the higher frequency can be estimated from the minimum and maximum source flux densities present in the initial 15.2-GHz sample, $S_{min}^{15.2}$ and $S_{max}^{15.2}$ (25 and 448 mJy), as $S_{min}^{15.2}/r_e$ and $S_{max}^{15.2}/r_e$, respectively.

We can also define a flux density, S_c, at the higher frequency above which our prediction might be less reliable. Because of the sparsity of sources in our lower frequency sample above the upper completeness limit, $S_c^{15.2}$, the measured count above $S_c^{15.2}/r_e$ could be less reliable because the measured spectral-index distribution may not be valid for sources with flux densities greater than this value. The respective values of S_{min} and S_{max} are calculated to be 15 and 266 mJy. We note that there are a few sources in our sample with $S_{15.2} \gtrsim 100$ mJy, which implies that $S_c \approx 60$ mJy.

An alternative approach, which in practice yields similar results, uses some further knowledge of the source count at the lower frequency. AMI Consortium: Davies et al. (2011) found that the 15.7-GHz differential source count increases less steeply below ≈ 2 mJy. Similarly, we know from 20-GHz source count measurements by Massardi et al. (2011) that the 9C power-law parametriza-tion is unlikely to provide a good description of the source count above ~ 1 Jy at the lower frequency; the 9C survey data did not sample the source count at such high flux densities, since there were no sources with $S_{15.2} > 1$ Jy within the survey areas.

Assuming that there are no sources with spectral indices < -0.56 (the most negative spectral index measured for a source in our sample), the lower flux density limit above which our estimated count is valid at 93.2 GHz is ≈ 2 mJy $\times (93.2/15.2)^{+0.56} \approx 6$ mJy. Similarly, assuming that there are no sources with spectral indices > 1.42 (the largest value measured), the upper flux density limit at the higher frequency is ~ 1 Jy $\times (93.2/15.2)^{-1.42} \sim 100$ mJy. For this second approach, we have assumed that our measured spectral-index distribution (or at least the most extreme values of the distribution) is valid for sources with $2 \lesssim S_{15.2} \lesssim 1000$ mJy.

The two approaches indicate that our high-frequency prediction is likely to be most accurate for $10 \lesssim S_{93.2} \lesssim 100$ mJy. The prediction may be useful outside of this range but, here, must be treated with caution.

8.2 Comparison with results of Waldram et al. (2007)

Fig. 2 shows the 93.2-GHz source count prediction made here, along with a number of other 90-GHz-band source count predictions. As indicated by the figure, the 90-GHz source count estimated by Waldram et al. (2007) is significantly lower than our prediction, having an estimated K parameter of 0.25 ± 0.05.
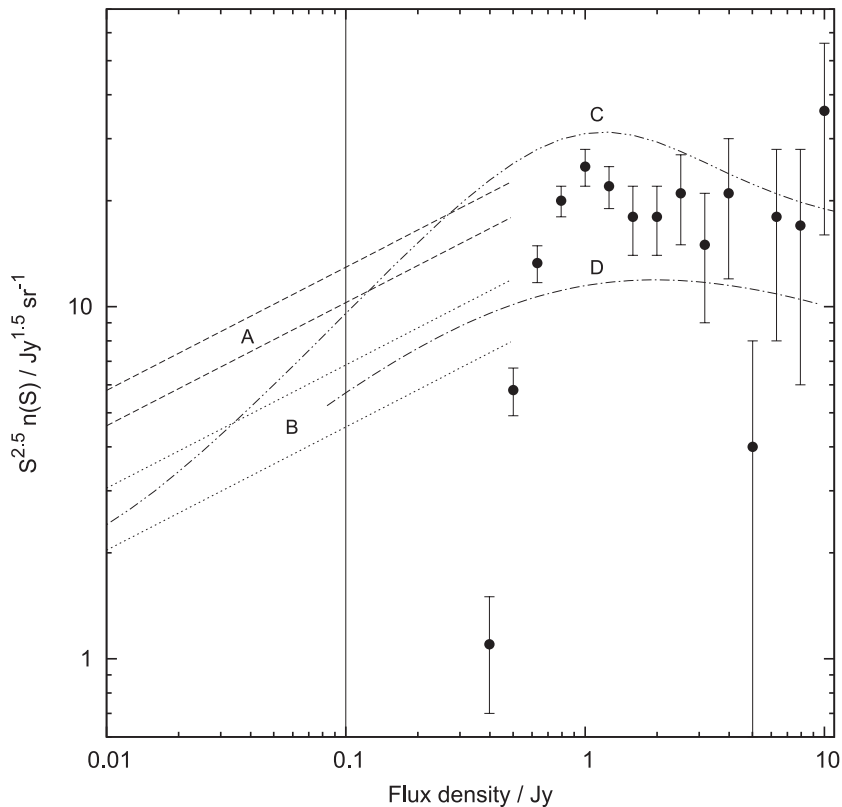

Figure 2. Normalised ($S^{2.5}n(S) = S^{2.5}\frac{dN}{dS}$) 90-GHz-band differential source counts. The dashed lines (straddling marker A) show the uncertainty in our prediction for 93.2 GHz. The dotted lines (straddling marker B) show the bounds of the 90-GHz Waldram et al. (2007) estimate. Although we have plotted these projections up to $S = 500$ mJy, we stress that they are likely to be most accurate for $S \lesssim 100$ mJy – we have indicated this value using a solid vertical line. The double dot–dashed line (labelled C) shows the 93-GHz model prediction by de Zotti et al. (2005). The dot–dashed line (labelled D) shows the 95-GHz estimate of Sadler et al. (2008). The circles show the 100-GHz count measured by Planck collaboration (2011); the count drops off rapidly for $S \lesssim 900$ mJy owing to incompleteness in this flux density range.

To make their 90-GHz source count prediction, Waldram et al. used results from simultaneous, multifrequency observations by Bolton et al. (2004) of a complete sample of 9C sources carried out using the VLA and RT. The data were collected at 4.8, 22 and 43 GHz using the VLA and at 15.2 GHz using the RT; 90-GHz flux density estimates were derived for the sources by extrapolation from the observed, 15-, 22- and 43-GHz flux densities.

The discrepancy between our source count prediction and that of Waldram et al. has led us to re-assess the accuracy of the 43-GHz flux density scale used by Bolton et al. In a forthcoming paper (Bolton et al., in preparation) we show that the 43-GHz flux densities measured using the VLA are up to 40 per cent lower than the values expected by extrapolation of the source flux densities observed at frequencies <43 GHz. In the light of this, the forthcoming paper will also contain a re-evaluation of the Waldram et al. source count estimates. For instance, the value of K obtained by simply omitting the 43-GHz data points from the analysis is much more consistent with the value presented in this paper.

8.3 Comparison with results of Sadler et al. (2008)

Fig. 2 indicates that the 95-GHz source count prediction by Sadler et al. (2008) is in much closer agreement, over the common range of validity (around 100 mJy), with the Waldram et al. (2007) estimate than with our projection here. Sadler et al. made their 95-GHz source count prediction using a method, developed by Kellermann (1964), similar to that used in this paper. The authors used the Australia Telescope Compact Array to carry out simultaneous 20- and 95-GHz observations of a flux-density-limited sample of sources, originally detected as part of the Australia Telescope 20-GHz (AT20G) survey (Ricci et al. 2004; Sadler et al. 2006); the sample comprised of 70 sources with $S_{20} > 150$ mJy.

Fig. 3 shows the measured 15.7-to-93.2-GHz spectral-index distribution for our sample and the 20-to-95-GHz distribution for the Sadler et al. sample. For both samples, three sources were not detected at the higher frequency; the shaded areas in the figure represent the upper limits of the spectral indices of these sources.

The typical lower frequency flux density of the sources in the two samples is quite different. The median 20-GHz flux density for sources in the Sadler et al. sample is ≈270 mJy; the sources in our sample have a median 15.7-GHz flux density of ≈45 mJy – a factor of 6 smaller. Despite this difference, the distributions for the samples are fairly similar. The 9C sample has a somewhat broader distribution and the sources belonging to this sample have a slightly steeper typical spectral index – they have a median spectral index of 0.54 compared to a value of 0.39 for sources belonging to the AT20G sample. However, these small differences cannot explain the significant difference between the two source count predictions.

The discrepancy between the two predictions appears, instead, to be attributable to the difference between the lower frequency source counts from which the extrapolations were made. Fig. 4 shows the 9C source count extrapolated to 20 GHz compared with the 20-GHz source count used by Sadler et al. (2008) in making their high-frequency prediction, as well as the most recent AT20G source count (Massardi et al. 2011). The projection of the 9C count to 20 GHz was made using the method described in Section 6.1 – it was simply assumed that the measured 15.7-to-93.2-GHz spectral indices are identical to those between 15.2 and 20 GHz.

The figure indicates that the original AT20G source count is significantly lower than the 20-GHz count predicted using the 9C data. However, it also shows that the most recent AT20G count is in much better agreement with our predicted 20-GHz count.
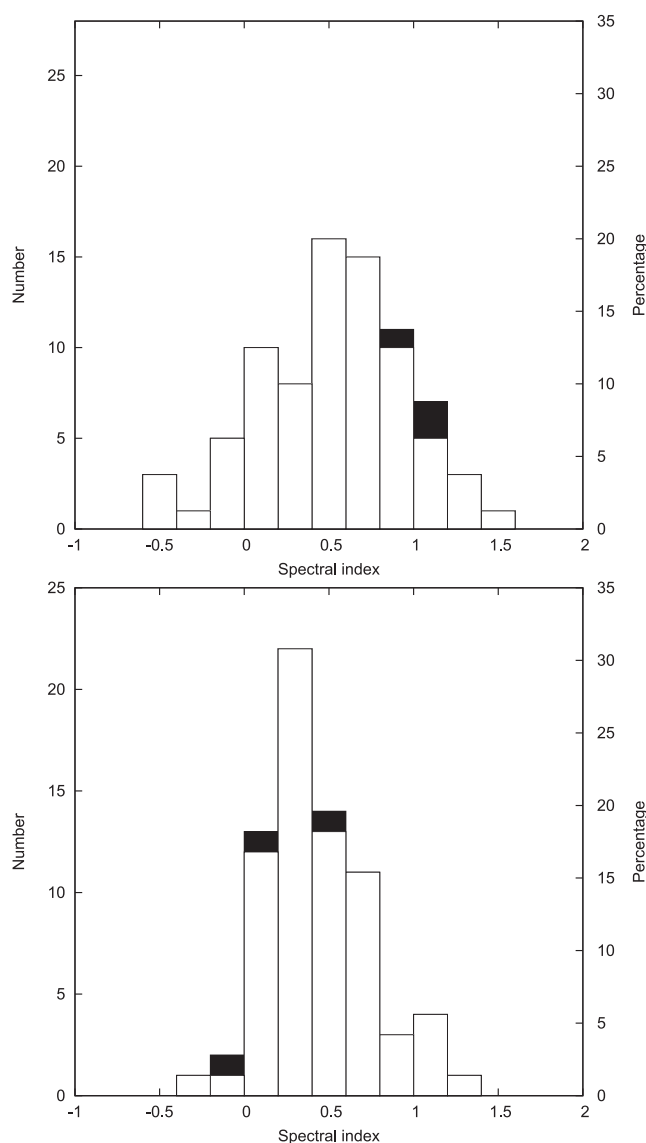

Figure 3. Histograms showing (top) the 15.7-to-93.2-GHz spectral-index distribution from the AMI and CARMA observations described in this paper and (bottom) the 20-to-95-GHz spectral-index distribution for the flux-density-limited sample of Sadler et al. (2008). The shaded regions represent limiting spectral indices for sources that were not detected at the higher frequencies.

The original AT20G count was subject to significant uncertainty, which has been substantially reduced as the survey has proceeded and more data have been gathered. Presumably, the 90-GHz-band source counts predicted using the revised AT20G count would be in much better agreement with our estimated count than those of Sadler et al. (2008).

As an additional check, the K value for 22 GHz (compared to 15.2 GHz) was estimated using our data – again it was assumed that the measured 15.7-to-93.2-GHz spectral indices hold over the frequency range of interest. The K value was calculated as 0.81, which is similar to the value of 0.80 calculated by Waldram et al. (2007) on the basis of direct 15.2- and 22-GHz measurements. The similarity of the values provides a hint that there is little spectral steepening between 22 and 93.2 GHz. This stands in contrast to a recent work by Sajina et al. (2011), who find some evidence for spectral steepening
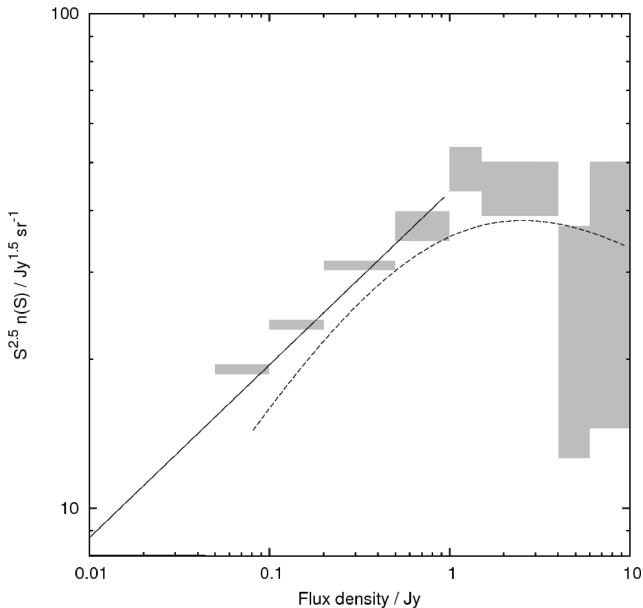
Figure 4. 20-GHz-band, normalized, differential source counts. The solid line indicates the 20-GHz count predicted using the 9C source count and the 15.7-to-93.2-GHz spectral indices presented in this paper. The dashed line shows the AT20G count, used by Sadler et al. (2008) to make their high-frequency source count prediction. The shaded boxes indicate the most recent measured AT20G source count, presented by Massardi et al. (2011). The sizes of the boxes parallel to the flux density axis represent the widths of the bins used in deriving the count. The uncertainty in the counts is shown by the sizes of the boxes in the perpendicular direction.

between 43 and 90 GHz in a sample of sources originally detected as part of the AT20G survey – however, the typical flux density of the sources in their sample is significantly higher than that of our sample.

8.4 Comparison with the de Zotti et al. (2005) model

Predictions for high-frequency radio source counts over a wide range of frequencies and flux densities have been made by de Zotti et al. (2005). Fig. 2 shows their model source count at 93 GHz. As indicated by the figure, the de Zotti et al. prediction is significantly lower than our prediction over the flux density range for which we believe our projection to be most accurate. For instance, at $S = 50$ mJy our differential source count estimate is $\approx$1.65 times that predicted by de Zotti et al. – at 10 mJy this factor is $\approx$2.3.

Unfortunately, the lower limits on the 93.2-GHz count, discussed in Section 7, do not help to discriminate between the two predictions, as they all lie below the de Zotti et al. estimate. However, at higher flux densities, we are able to compare the de Zotti et al. model to the *Planck* data. Since the 100-GHz version of the de Zotti et al. model is barely distinguishable from the 93-GHz version over the flux density range plotted, given the scale used for Fig. 2, we can simply compare to the 93-GHz model line. At the highest flux densities the model count is in relatively good agreement with the measured values, given the uncertainties. However, at slightly lower flux densities, the *Planck* points are systematically below the model prediction.

9 CONCLUSIONS

We have carried out close-to-simultaneous 15.7- and 93.2-GHz follow-up observations, using the AMI LA and CARMA, respectively, for a sample of 80 sources, originally detected at 15.2 GHz as part of the 9C survey. The sources form two complete samples at 15.2 GHz. Of the 80 sources, 77 were detected at the higher frequency. The measured 15.7-to-93.2-GHz spectral-index distribution indicates that the majority of the sources in the sample have falling or gently rising spectra, with only a few more steeply rising spectra sources; the median spectral index for the sample is 0.54. The spectral properties of the sample are similar to those measured by Sadler et al. (2008) for their 20-GHz-selected sample; they measured a median 20-to-95-GHz spectral index of 0.39 for sources in their sample, which has a somewhat higher typical flux density than our sample.

The measured spectral-index distribution has been used to extrapolate the 9C source count to 93.2 GHz, for which our estimated differential source count is $26 \pm 4(S/\text{Jy})^{-2.15}$ Jy^{-1} sr^{-1}. We believe our prediction to be most accurate for $10 \lesssim S \lesssim 100$ mJy.

The estimated differential count is more than two times higher than the 90-GHz estimate of Waldram et al. (2007). This has led us to re-assess the 43-GHz flux density scale used by Bolton et al. (2004), on which the Waldram et al. estimates rely, and to re-evaluate those predictions – this work will be presented in a forthcoming paper (Bolton et al., in preparation). In summary, we believe that the 43-GHz flux densities were too low, which, in turn, affected the 90-GHz projection.

Our source count estimate is significantly higher than that of Sadler et al. (2008) over the common flux density range of the predictions (around 100 mJy). The Sadler estimate is based on extrapolation of the count at 20 GHz: we note that the most recent AT20G count (Massardi et al. 2011) is significantly higher than the older count used in the Sadler et al. (2008) work. Indeed, when we use our measured spectral-index distribution to extrapolate the 9C count to 20 GHz, we find it to be in much better agreement with the Massardi et al. (2011) AT20G count than with that used in making the Sadler et al. prediction.

At higher flux densities $S \gtrsim 1$ Jy, where our prediction is not valid, the picture is, again, rather messy. The 100-GHz source counts of Planck collaboration (2011) lie above the estimate of Sadler et al. (2008) but below that of de Zotti et al. (2005).

The picture ought to become clearer with the arrival of the revised Waldram et al. prediction and with further projections based on follow-up observations of AT20G samples, which will, hopefully, serve to tie together the lower and higher flux density predictions.

REFERENCES

AMI Consortium: Davies M. L. et al., 2009, MNRAS, 400, 984
AMI Consortium: Davies M. L. et al., 2011, MNRAS, 415, 2708
AMI Consortium: Franzen T. M. O. et al., 2011, MNRAS, 415, 2699
AMI Consortium: Zwart J. T. L. et al., 2008, MNRAS, 391, 1545
Barreiro R. B., Martínez-González E., Vielva P., Hobson M. P., 2006, MN-RAS, 368, 226
Bolton R. C. et al., 2004, MNRAS, 354, 485
Condon J. J., 1984, ApJ, 287, 481
de Zotti G., Ricci R., Mesa D., Silva L., Mazzotta P., Toffolatti L., González-Nuevo J., 2005, A&A, 431, 893
de Zotti G., Massardi M., Negrello M., Wall J., 2010, A&AR, 18, 1
Kellermann K. I., 1964, ApJ, 140, 969
Knox L., Holder G. P., Church S. E., 2004, ApJ, 612, 96
Massardi M., Bonaldi A., Bonavera L., López-Caniego M., de Zotti G., Ekers R. D., 2011, MNRAS, 412, 318
Planck collaboration: Ade P. A. R. et al., 2011, A&A, 536, 13
Ricci R. et al., 2004, MNRAS, 354, 305
Rodríguez L. F., Gómez Y., Tafoya D., 2007, ApJ, 663, 1083
Sadler E. M. et al., 2006, MNRAS, 371, 898
Sadler E. M., Ricci R., Ekers R. D., Sault R. J., Jackson C. A., de Zotti G., 2008, MNRAS, 385, 1656
Sajina A., Partridge B., Evans T., Stefl S., Vechik N., Myers S., Dicker S., Korngut P., 2011, ApJ, 732, 45
Sault R. J., Teuben P. J., Wright M. C. H., 1995, in Shaw R., Payne H. E., Hayes J. J. E., eds, ASP Conf. Ser. Vol. 77, A Retrospective View of Miriad in Astronomical Data Analysis Software and Systems IV. Astron. Soc. Pac., San Francisco, p. 433
Tafoya D., Gómez Y., Rodríguez L. F., 2004, ApJ, 610, 827
Waldram E. M., Pooley G. G., Grainge K. J. B., Jones M. E., Saunders R. D. E., Scott P. F., Taylor A. C., 2003, MNRAS, 342, 915
Waldram E. M., Bolton R. C., Pooley G. G., Riley J. M., 2007, MNRAS, 379, 1442
Waldram E. M., Pooley G. G., Davies M. L., Grainge K. J. B., Scott P. F., 2010, MNRAS, 404, 1005
Watson R. A. et al., 2003, MNRAS, 341, 1057
Weiland J. L. et al., 2011, ApJS, 192, 19

This paper has been typeset from a TEX/LATEX file prepared by the author.